Radiogenic p-isotopes from SN Ia, nuclear physics uncertainties and Galactic chemical evolution compared with values in primitive meteorites

C. Travaglio[1]

INAF - Astrophysical Observatory Turin, Strada Osservatorio 20, 10025 Pino Torinese (Turin), Italy

B2FH Association - Turin, Italy

travaglio@oato.inaf.it, claudia.travaglio@b2fh.org

R. Gallino[2]

Dipartimento di Fisica, Universitá di Torino, Via P.Giuria 1, 10125 Turin, Italy

B2FH Association - Turin, Italy

T. Rauscher[3]

Centre for Astrophysics Research, School of Physics, Astronomy and Mathematics, University of Hertfordshire, Hatfield AL10 9AB, United Kingdom

N. Dauphas[4]

Origins Laboratory, Department of the Geophysical Sciences and Enrico Fermi Institute, The University of Chicago, Chicago, IL 60637, USA

F. K. Röpke[5]

Universität Würzburg, Am Hubland, D-97074 Würzburg, Germany

and

W. Hillebrandt[6]

Max-Planck-Institut für Astrophysik, Karl-Schwarzschild-Str. 1, D-85748 Garching bei München, Germany

Received ______________; accepted ______________

ABSTRACT

The nucleosynthesis of proton-rich isotopes is calculated for multi-dimensional Chandrasekhar-mass models of Type Ia supernovae with different metallicities. The predicted abundances of the short-lived radioactive isotopes ^{92}Nb, ^{97,98}Tc, and ^{146}Sm are given in this framework. The abundance seeds are obtained by calculating *s*-process nucleosynthesis in the material accreted onto a carbon-oxygen white dwarf from a binary companion. A fine grid of *s*-seeds at different metallicities and ^{13}C-pocket efficiencies is considered. A galactic chemical evolution model is used to predict the contribution of SN Ia to the solar system *p*-nuclei composition measured in meteorites. Nuclear physics uncertainties are critical to determine the role of SNe Ia in the production of ^{92}Nb and ^{146}Sm. We find that, if standard Chandrasekhar-mass SNe Ia are at least 50% of all SNIa, they are strong candidates for reproducing the radiogenic *p*-process signature observed in meteorites.

Subject headings: hydrodynamic, supernovae, nucleosynthesis, *p*-process, radiogenic, meteorites, chemical evolution

1. Introduction

The astrophysical p-process is the conversion of a s- or r-process distribution into proton-rich nuclei via photodisintegration reactions and charged particle reactions. This conversion can only occur on a hydrodynamical timescale when the temperature is higher than 10^9 K. Core-collapse supernovae (ccSN in what follows) and/or Type Ia supernovae (SNe Ia hereafter) are the most probable contributors to the bulk of the solar system p-nuclei (for ccSN see, *e.g.*, Howard & Meyer 1993, Rauscher et al. 2002; for SN Ia see *e.g.*, Travaglio et al. 2011 hereafter TRV11, Kusakabe et al. 2011, Arnould & Goriely 2006).

p-process nucleosynthesis occurs in SNIa by processing matter that was enriched in s-process seeds during pre-explosive evolution of the SNIa progenitor. Therefore, it is essential to determine the s-process enrichment in the exploding white dwarf (WD hereafter). We consider a binary system, accreting material from a giant star onto the WD. We explore the single-degenerate scenario with a Chandrasekhar mass carbon-oxygen (CO-) WD. The s-process seeds are assumed to be produced from a sequence of thermal pulse instabilities in the accreted material. This idea was described in detail by TRV11 and Kusakabe et al. (2011), and previously discussed by Iben (1981), Iben & Tutukov (1991), Howard & Meyer (1993). Recurrent flashes are assumed to occur in the He-shell during the accretion phase, resulting in enrichment of the CO-WD in s-nuclei . The mass involved in the ^{13}C-pocket (a tiny layer enriched in ^{13}C responsible for the production of s-process nuclei) is a free parameter of the model. Since no model exists for the production of s-seeds in the accretion phase, different s-seed distributions are explored in order to better understand the dependence of our results on the initial seed composition (see also the discussion in TRV11).

The p-process produces radiogenic isotopes with relatively long half-lives (Rauscher 2013). A number of now extinct short-lived nuclides were present in the early solar system. Their past presence in meteorites is revealed by measuring excesses of their decay-products in meteorites (Dauphas & Chaussidon 2011; Davis & McKeegan 2013).

The isotope ^{92}Nb decays with a half-life of 34.7 Myr to the stable nucleus ^{92}Zr via β decay. Harper (1996) found first evidence for live ^{92}Nb in the early solar system material by measuring a small excess of ^{92}Zr in rutile (TiO_2) extracted from the Toluca iron meteorite. Studies of supernova neutrino nucleosynthesis (Hayakawa et al. 2013), alpha-rich freezeout (Meyer 2003), or γ-process (Dauphas et al. 2003), tried to explain the observed abundance of meteoritic ^{92}Nb. Nevertheless, the astrophysical site where the solar system ^{92}Nb was made is still uncertain.

The isotope ^{146}Sm decays to the stable isotope ^{142}Nd by α-emission. Prinzhofer et al. (1989, 1992) and Lugmair & Galer (1992) provided the first solid estimates of the initial abundance of ^{146}Sm at the birth of the solar system. The half-life of ^{146}Sm is still under debate. The first measurements of its half-life was performed by Friedmann (1966) and later confirmed by Meissner et al. (1987), setting a value of 103 ± 5 Myr. More recently Kinoshita et al.(2012), based on an analysis of ^{146}Sm/^{147}Sm α-activity and atom ratios, redetermined the half-life of ^{146}Sm and found 68 ± 7 Myr.

The isotopes ^{97}Tc ($t_{1/2} = 4.21$ Myr) and ^{98}Tc ($t_{1/2} = 4.2$ Myr) are of p-origin and may have been present in the early solar system but meteorite measurements only provide upper-limits on the abundances of these short-lived nuclides (Dauphas et al. 2002; Becker & Walker 2003).

In this work, we discuss the productions of ^{92}Nb, ^{97,98}Tc, and ^{146}Sm under SN Ia conditions, their dependence on the astrophysical environment, on the initial metallicity of the star, and on nuclear physics quantities.

In Section 2, the SN Ia model and the method to compute nucleosynthesis in multi-D

SN Ia (TRV11 and references therein) are presented. In Section 3 the p-process calculations for radioactive isotopes and their dependence on metallicity and s-seeds are discussed. In Section 4 the galactic chemical evolution model (Travaglio et al. 2004; Travaglio et al. 1999) together with calculations for radioactive p-isotopes are presented. Finally, in Section 5 the sensitivity of ^{146}Sm and ^{92}Nb SNIa yields to the uncertainties on rates as well as on their lifetimes are discussed.

2. Type Ia supernova nucleosynthesis and p-process radioactivities.

For the SN Ia explosions, we use a delayed detonation model (DDT-a) based on 2-dimensional simulations of Kasen et al. (2009) and described in detail in TRV11. The scenario considered for SNIa is that of single-degenerate star, in which the WD accretes material from a main-sequence or evolved companion star. Nucleosynthesis is calculated in a post-processing scheme making use of tracer-particle methods (as described in detail in TRV11 and Travaglio et al. 2004b). For each tracer, explosive nucleosynthesis is followed using a detailed nuclear reaction network for all isotopes up to ^{209}Bi. The nuclear reaction rates used are based on the experimental values and the Hauser & Feshbach statistical model NON-SMOKER (Rauscher & Thielemann 2000), including the experimental results of Maxwellian averaged neutron-capture cross sections of various p-only isotopes (Dillmann et al. 2010; Marganiec et al 2010). Theoretical and experimental electron capture and β-decay rates are from Langanke & Martínez-Pinedo (2000).

TRV11 demonstrated that the abundances of the p-nuclei in SNIa strongly depend on the s-seeds assumed. However, the ratio of a radiogenic isotope to the neighbor stable p-isotope (i.e. ^{92}Nb/^{92}Mo, ^{97,98}Tc/^{98}Ru and ^{146}Sm/^{144}Sm), is less dependent of the assumptions made for the s-seeds. Note that all the reference stable isotopes are pure p-nuclei also.

The abundances of ^{92}Nb, ^{92}Mo, ^{97,98}Tc,^{98}Ru and ^{146}Sm,^{144}Sm obtained in this way are plotted in Figs. 1−3 for tracers selected in the peak temperature range that allows p-process nucleosynthesis (*i.e.*, $1.5 - 3.7$ GK). Each dot represents one tracer at its peak temperature. In the DDT-a model, we have 51200 tracer particles in total, and 4624 of them in the p-process temperature range located in the accreted mass, representing a total mass of 0.127 $M_\odot$ (the mass of a single tracer is 2.75×10^{-5} $M_\odot$). Since we verified that an important contribution to ^{146}Sm comes from the decay of ^{150}Gd and of ^{154}Dy, we did not include them directly in the ^{146}Sm abundance plotted but they are shown separately in Fig. 3. As can be seen in Fig. 1, most of the production of ^{92}Nb takes place at around $T = 2.5 - 2.7$ GK, where ^{20}Ne burning occurs (see Figure 5 in TRV11 for details).

s-process distributions are calculated for a fine grid of metallicities, *i.e.*, $Z = 0.02, 0.015, 0.012, 0.010, 0.006, 0.003$, and for different ^{13}C-pockets (ST×2, ST×1.3, ST, ST/1.5, where $\sim 4 \times 10^{-6}$ $M_\odot$ of ^{13}C in the pocket corresponds to the ST case, Gallino et al. 1998). The mass involved and the profile of the ^{13}C mass fraction are treated as free parameters. In the present state of the art, there is no model that can predict s-process nucleosynthesis during the mass-accretion phase prior a CO-WD explosion. TRV11 presented and discussed different possible s-process seed distributions in mass-accretion conditions, and their consequences for p-process nucleosynthesis. Here and in Travaglio et al. (2014, in prep.), we add a detailed analysis of the dependence on metallicity.

The goal of the present work is to provide predictions for solar composition of radioactive p-nuclei. The Galactic chemical evolution code used has been presented already in previous studies (Travaglio et al. 1999, 2001, 2004, Bisterzo et al. 2014), see Section 4 for a detailed discussion.

3. p-process and radioactive ^{92}Nb, ^{97,98}Tc, and ^{146}Sm for different metallicities

Extinct radionuclides were found in meteorites (Dauphas & Chaussidon 2011; Davis & McKeegan 2013) and some of them are p-only radiogenic nuclei, *i.e.*, ^{92}Nb and ^{146}Sm. Their signatures were detected as an excess abundance of the daughter nuclei (^{92}Zr and ^{146}Nd).

Whereas ^{93}Nb is 85% s-process and 15% r-process (Arlandini et al. 1999), ^{92}Nb is an important isotope since it is produced by the γ-process but is completely shielded from contributions from rp- or νp-processes (Dauphas et al. 2003), and as such can help test models of p-process nucleosynthesis. Meteorite measurements show that this nuclide was present at the birth of the solar system (with an initial ^{92}Nb/^{92}Mo ratio of $(2.80\pm0.5)\times10^{-5}$ (Harper 1996; Schönbächler et al. 2002; Rauscher et al. 2013). Nevertheless its astrophysical production site is still unknown (Dauphas et al. 2003; Meyer 2003). Note that ^{92}Nb is normalized to ^{92}Mo because both are p-process nuclides while ^{93}Nb is mainly a s-process isotope (by the radiogenic decay of ^{93}Zr).

The underproduction of ^{92,94}Mo and ^{96,98}Ru in the γ-process could, in principle, be compensated by contributions of the rp- or νp-processes but this would lead to a too low ^{92}Nb/^{92}Mo ratio at solar system birth (Dauphas et al. 2003). Various theoretical estimates for the ratio ^{92}Nb/^{92}Mo are available in literature, for both SN Ia (Howard et al. 1991; Howard & Meyer 1993) and core-collapse supernovae (ccSN) (Woosley & Howard 1978; Woosley & Howard 1990; Rayet et al. 1995; Hoffman et al. 1996; Rauscher et al. 2002; Hayakawa et al. 2013). Some of these models can reproduce the solar system ^{92}Nb/^{92}Mo ratio but at the same time, they underproduce the amount of ^{92}Mo present in cosmic abundances, so they are unlikely contributors to p-process nuclides in the Mo-Ru mass region (Rauscher et al. 2002).

The short-lived ^{146}Sm was also present in meteorites at the birth of the solar system. The first attempts to estimate the ^{146}Sm/^{144}Sm ratio were published by Lugmair &

Marti (1977) and by Jacobsen & Wasserburg (1984). The initial ^{146}Sm/^{144}Sm ratio was constrained in meteorites by Lugmair & Galer (1992) and by Prinzhofer et al. (1992). A later study of eucrite meteorites by Boyet et al. (2010) confirmed the value found but improved the precision, contraining the ^{146}Sm/^{144}Sm ratio at the birth of the solar system to 0.0084 ± 0.0005 using a half-life of 103 Myr to correct for decay between formation of the eucrites and the solar system. Using the half-life for ^{146}Sm of 68 Myr and the last meteorite measurements, Kinoshita et al. (2012) estimated that the initial ^{146}Sm/^{144}Sm ratio was 9.4 $\pm$ 0.5 $\times$ 10^{-3}. Because eucrite crystallization occurred shortly after the formation of the solar system, the correction of the initial ^{146}Sm/^{144}Sm ratio is small and does not depend much on which ^{146}Sm half-life is used.

The nuclides ^{97,98}Tc have not been detected in meteorites yet, and only upper limits were derived. Dauphas et al. (2002) provided an upper-limit on the ^{97}Tc/^{98}Ru ratio of $<$ 4×10^{-4}. Becker & Walker (2003) provided an upper-limit on the ^{98}Tc/^{98}Ru ratio of $< 2\times 10^{-5}$.

In Table 1 we show the values of the radiogenic ratios ^{92}Nb/^{92}Mo, ^{97,98}Tc/^{98}Ru, and ^{146}Sm/^{144}Sm obtained with the tracer-particle nucleosynthesis calculations based on the DDT-a model as a function of metallicity. *s*-process distributions are calculated for a range of galactic disk metallicities, from solar value down to $Z = 0.003$. The effect of using different ^{13}C-pocket sizes is also explored (ST$\times$2, ST$\times$1.3, ST, ST/1.5, where $\sim 4 \times 10^{-6} M_{\odot}$ of ^{13}C in the pocket corresponds to the ST case, Gallino et al. 1998). The parameter used for Table 1 is ST$\times$1.3. The GCE calculations and comparisons with meteoritics abundances are described in details in the following section.

4. Galactic chemical evolution

The initial ^{92}Nb/^{92}Mo and ^{146}Sm/^{144}Sm ratios at the birth of the solar system are known from meteorite measurements. In order to compare these values with our model results, one has to use a model of chemical evolution of the Galaxy, as the abundances in the ISM at any given time reflect the interplay between production in stars and decay in the ISM. Note that we do not consider any contribution from stars other than SNIa to the nucleosynthesis of p-nuclides.

The Galactic chemical evolution code used here was presented in several publications (Travaglio et al. 1999; Travaglio et al. 2001; Travaglio et al. 2004; Bisterzo et al. 2014). It models the Galaxy as three interconnected zones; halo, thick disk, and thin disk. The evolution of the Galaxy is computed up to the present epoch ($t_{\rm today}$ = 13.8 Gyr, updated by WMAP, Bennet et al. 2013) and the solar system formation is assumed to have occurred 4.6 Gyr ago. Therefore the time corresponding to the birth of the solar system is $t_{\odot} = 9.2$ Gyr. Solar abundances are taken from Lodders et al. (2009) and massive star yields are from Rauscher et al. (2002). Iron is mostly produced by long-lived SNe Ia (a knee in the trend of [O/Fe] vs. [Fe/H] indicates the delayed contribution to Fe by SNe Ia, see e.g. McWilliam 1997). Following the common idea that oxygen is mainly synthesized by short-lived massive stars in ccSN and Fe is mostly produced by long-lived binary systems in the form of SNe Ia, the knee in the observed trend of [O/Fe] vs [Fe/H] (in field stars at different metallicities) indicates the delayed contribution to iron by SNe Ia (1/3 of Fe is probably produced by ccSN and 2/3 by SN Ia). As recently shown by Bisterzo et al. (2014), with an updated compilation of spectroscopic data, our model fits well the knee observed, giving a good constraint to the rate of ccSN *vs.* SN Ia, as well as to the treatment of binary stars included in the GCE code (for details see Travaglio *et al.* 1999).

The matrix of isotopes within the chemical evolution code was set to cover all the light nuclei up to the Fe-group, and all the heavy nuclei along the s-process and p-process paths up to ^{209}Bi. The resulting p-process production factors taken at the epoch of solar system formation for nuclei in the atomic mass number range $70 \leq A \leq 210$ are shown in detail in Travaglio et al. (2014, in prep.), with a fine grid of metallicities and exploring different s-process seed distributions. In this paper, the choice for s-seed distribution versus metallicity is discussed in detail, *i.e.*, we choose higher ^{13}C for higher metallicities (ST$\times$2 for solar metallicity, ST$\times$1.3 for metallicities down to 0.01, ST for $Z = 0.006$, and ST/1.5 for the lowest metallicities). The grid of metallicities used for the present work is described in Section 3 (see also Table 1). With this choice, the predicted ratios at 9.2 Gyr are ^{92}Nb/^{92}Mo $= 1.752 \times 10^{-5}$ (about a factor of 1.6 below the meteoritic value of $2.8 \pm 0.5 \times 10^{-5}$), ^{146}Sm/^{144}Sm $= 6.989 \times 10^{-3}$ (about a factor of 1.3 below the meteoritic value of $9.4 \pm 0.5 \times 10^{-3}$), ^{97}Tc/^{98}Ru $= 4.077 \times 10^{-5}$, and ^{98}Tc/^{98}Ru $= 6.471 \times 10^{-7}$ (for Tc the ratios measured in meteorites are upper limits). The ratios as a function of the age of the Galaxy (or of the metallicity) are given in Table 2. The meteoritic values measured and their errors are also reported in the same table . A detailed analysis and discussion on the importance of uncertainties of reaction rates for ^{92}Nb and ^{146}Sm is presented in the next section.

Most previous studies dealing with radioactive nuclides in meteorites have relied on analytical or semi-analytical approaches to predict the abundances of these nuclides in the ISM at solar system birth (Schramm & Wasserburg 1970; Clayton 1988; Dauphas et al. 2003; Dauphas 2005; Huss et al. 2009; Jacobsen 2005). The main virtue of these analytical approaches is that they allow one to rapidly explore the parameter space while capturing some of the most important features of galactic chemical evolution. However, this simplicity is achieved at the expense of realisticness. Analytical approaches can take into account the secondary nature of some nuclides, the fact that the galactic disk probably grew by infall of low-metallicity gas, and the fact that the rate of star formation is not strictly linear with the gas surface density. However, all analytical models rely on the instantaneous recycling approximation, which assumes that material newly produced in stars is immediately returned to the ISM. This assumption is not correct for nucleosynthesis in SNIa, and would produce a factor of 2 to 4 higher values of the radiogenic ratios discussed above, but also wrong predictions of Fe at solar composition. More sophisticated galactic chemical models such as that presented here should be used.

5. Nuclear and half-life uncertainties

Figure 4 shows the reaction flow (*i.e.*, time-integrated flux) for a selected tracer producing ^{146}Sm and ^{144}Sm isotopes. As can be seen in the figure, the main flow from heavier nuclei is following the line defined by mass number $A = Z + 82$, with Z being the nuclear charge. The production ratio of ^{146}Sm/^{144}Sm mainly depends on the $(\gamma,\mathrm{n})/(\gamma,\alpha)$ branching at ^{148}Gd (and more weakly on similar branchings at ^{152}Dy and ^{156}Er). This is due to the fact that ^{146}Gd is neutron magic and, after the passage of the shock wave, decays to ^{146}Eu and then to ^{146}Sm. This was already pointed out by Woosley & Howard (1990) and further investigated by Rauscher et al. (1995) and Somorjai et al. (1998) for the γ-process in massive stars. This branching is independent of the seeds but a weak dependence of the ^{146}Sm/^{144}Sm ratio stems from the production of ^{144}Sm and the weak (γ,n) flow in Sm. This weak dependence is seen in Table 2, where the ^{146}Sm/^{144}Sm ratio obtained for different metallicities is shown and also in Table 3 where additionally the dependence on various ^{148}Gd$(\gamma,\alpha)^{144}$Sm rates is presented (also see discussion below).

Photodisintegration rates at high plasma temperature cannot be constrained by direct measurements (Rauscher 2012; Rauscher 2014). A better test of predicted reaction cross sections and astrophysical reaction rates could be obtained by experimentally determining capture cross sections. Since ^{147}Gd, however, is an unstable nucleus with a half-life of 38.06

hr, a measurement of ^{147}Gd(n,γ)^{148}Gd is not feasible and thus its rate has to be derived from Hauser-Feshbach theory. For the calculations shown here, the rate by Rauscher & Thielemann (2000) was used. Comparison to neutron capture data along the valley of beta-stability showed that the averaged uncertainty of the predictions was about 30% but local deviations up to a factor of 2 were possible (Rauscher et al. 1997; Rauscher et al. 2001; Rauscher 2012).

The measurement of the low-energy (α,γ) cross section of the stable ^{144}Sm nucleus by Somorjai et al. (1998) sets the stage for a long-standing puzzle regarding the prediction of low-energy α-capture and emission. The cross section was found to be lower by more than an order of magnitude than all predictions. Over the past years, many attempts have been made to construct improved α+nucleus optical potentials to explain these data (see, *e.g.*, Kiss *et al.* 2013; and Rauscher *et al.* 2013) and references therein. Recently, Rauscher (2013) suggested that including an additional reaction channel, only affecting α-capture but not emission, the experimental results can be reproduced. In Table 3, the ^{146}Sm/^{144}Sm ratios obtained with three different ^{148}Gd(γ,α)^{144}Sm rate predictions are shown: the original rate by Rauscher & Thielemann (2000) based on a cross section higher than the experimental value, the rate based on a fit to the Somorjai et al. (1998) (α,γ) cross sections, and the new rate by Rauscher (2013) which reproduces the measured cross sections but predicts a larger α-emission rate. In ccSN, the Rauscher & Thielemann (2000) rate gave a too low ^{146}Sm/^{144}Sm ratio compared to meteoritic values, the fit to Somorjai et al. (1998) gave a much larger ratio, while the new rate again provided a lower ratio due to the stronger α-emission (Rauscher 2013; Rauscher et al. 2013). All of these values were just barely compatible or incompatible with meteoritic ratios. For the SNIa case studied here, the final ^{146}Sm/^{144}Sm ratio integrated over the GCE is found to be compatible when using the rate fit by Somorjai et al. (1998) but also the new rate by Rauscher (2013). The difference with respect to the ccSN results is due to the different temperature history of the tracer in SN Ia as compared to the situation in a ccSN shock front, since the $(\gamma,\mathrm{n})/(\gamma,\alpha)$ branching at ^{148}Gd is temperature dependent. It should be noted that these ratios still bear an additional uncertainty from the ^{148}Gd(γ,n) rate, as discussed above.

All the calculations presented here used the most recent ^{146}Sm half-life of 68 Myr (Kinoshita et al. 2012). However, it is worth noting that the value of this half-life is still the subject of ongoing discussions as comparisons of ^{146}Sm-^{142}Nd with Pb-Pb or ^{147}Sm-^{143}Nd dating techniques may be more consistent with a longer half-life of 103 Myr (Borg et al. 2014). This half-life is important in early solar system chronology and it should be remeasured to ascertain its value.

The production of the radiogenic ^{92}Nb is governed by the destruction of ^{93}Nb and ^{92}Zr seeds, as can be seen from the flows in Fig. 5. It also gets some indirect contributions from ^{91,94,96}Zr via ^{92}Zr but none from ^{90}Zr. The nuclide ^{92}Nb is mainly destroyed by the reaction ^{92}Nb$(\gamma,\mathrm{n})^{91}$Nb, while two reactions produce it, ^{93}Nb$(\gamma,\mathrm{n})^{92}$Nb and ^{92}Zr(p,n)^{92}Nb. A minor production channel (about 3%) is ^{91}Zr$(\mathrm{p},\gamma)^{92}$Nb. Because the two reactions destroying ^{92}Zr – ^{92}Zr(p,n) and ^{92}Zr(p,γ) – both eventually lead to ^{92}Nb production, their relative magnitude is not important, only their combination into a total rate. The production of ^{92}Zr proceeds via (γ,n) sequences from the other Zr isotopes. The slowest reactions in these sequences are the ones removing a paired neutron and thus they dominate the timescale and the flow. Here, this is ^{94}Zr$(\gamma,\mathrm{n})^{93}$Zr and, with slightly less importance, ^{96}Zr$(\gamma,\mathrm{n})^{95}$Zr, both leading to eventual production of ^{92}Zr. Finally, ^{94}Nb$(\gamma,\mathrm{n})^{93}$Nb is important in the production of ^{93}Nb from neutron-richer Nb isotopes.

The rates of ^{94}Zr$(\gamma,\mathrm{n})^{93}$Zr and ^{94}Nb$(\gamma,\mathrm{n})^{93}$Nb are experimentally determined through their measured neutron capture cross sections (Kadonis, Dillmann et al. 2006). Despite of the elevated temperatures found in γ-process nucleosynthesis, the experimental data constrains both capture and photodisintegration well in these cases (Rauscher 2012). For the other rates given above, and their reverse reactions, we used predictions by Rauscher & Thielemann (2000) in our standard calculations. The ^{96}Zr(γ,n)^{95}Zr rate comes from a theory estimate as given in KADoNiS (Dillmann et al. 2006, Bao et al. 2000).

The uncertainty in the ^{92}Nb/^{92}Mo ratio also contains the uncertainty in the ^{92}Mo production. Figure 6 shows the time-integrated flows in the tracer that produces the main fraction of ^{92}Mo. The flow pattern is less complex than in the case of ^{92}Nb. The main contribution to this nuclide (about 50%) is through (γ,n) sequences coming from the stable Mo isotopes with mass numbers $A > 94$. These are mainly producing ^{94}Mo, part of which is converted to ^{92}Mo through the reaction sequence ^{94}Mo(γ,n)^{93}Mo(γ,n)^{92}Mo. The slower reaction in this sequence, determining the flow is ^{94}Mo(γ,n)^{93}Mo, leaving an unpaired neutron in ^{93}Mo. The second important path, contributing about 35%, is the sequence ^{93}Nb(p,n)^{93}Mo(γ,n)^{92}Mo. Although the magnitude of the (p,n) reaction also scales with the proton density, the ^{93}Mo(γ,n)^{92}Mo reaction is the faster one again in this sequence at our SNIa conditions. Finally, the reaction ^{91}Nb(p,γ) provides a small (15%), additional contribution to ^{92}Mo. There are only theoretical predictions for the rates that are important, ^{94}Mo(γ,n)^{93}Mo, ^{93}Nb(p,n)^{92}Mo, and (with lower impact) ^{91}Nb(p,γ)^{92}Mo. The ^{92}Mo production would scale according to the above weights when new rate determinations become available for these reactions.

The important theoretically estimated rates affecting the production of ^{92}Nd and ^{92}Mo are summarized in Table 4. In order to check the uncertainty in our GCE calculations at the solar system birth for the ^{92}Nb/^{92}Mo ratio due to uncertainties in the reaction rates, we varied the most important rates found above by a factor of two. Calculations with two rate sets were performed, probing the extremal values expected for the ^{92}Nb/^{92}Mo ratio as indicated in Table 4. This leads to a ^{92}Nb/^{92}Mo ratio at 9.2 Gyr varying from 1.660×10^{-5} for the *Rate set MIN* up to 3.118×10^{-5} for the *Rate set MAX* (the results are summarized in the last line of Table 4).

As shown in Table 2, the SNIa yields calculated here, when folded in a galactic chemical evolution, given nuclear physics uncertainties, we can reproduce the ^{92}Nb/^{92}Mo and ^{146}Sm/^{144}Sm ratios at solar system birth measured in meteorites (^{92}Nb/^{92}Mo $= 2.8 \times 10^{-5}$ in meteorites *vs.* $1.8{\times}10^{-5}$ predicted; (^{146}Sm/^{144}Sm $= 9.4 \times 10^{-3}$ in meteorites *vs.* $7.0{\times}10^{-3}$ predicted). Note that the match between predicted and measured ratios requires that the material that made the solar system had not been isolated from fresh nucleosynthetic inputs for some extended time, as is observed for some r-process short-lived nuclides such as ^{129}I (Qian et al. 1998). These authors concluded that the discrepancy can be solved if some r-process isotopes are produced in rare events only. This study supports the view that single-degenerate SNIa may be important contributors to the nucleosynthesis of p-process nuclides in the Galaxy.

6. Conclusions

In this work we discuss the production of short-lived radionuclides ^{92}Nb, ^{146}Sm and ^{97,98}Tc by single degenerate SNIa stars. Using a simple Galactic chemical evolution code, we show that a significant fraction of p-process extinct radionuclides ^{92}Nb, ^{146}Sm, and ^{96,98}Tc in meteorites could have been produced by the γ-process in SNeIa.

Travaglio et al. (2011) showed that SNIa were likely sites for p-process nucleosynthesis. In particular, enrichment in s-seeds during the pre-explosive evolution leads to the production of ^{92}Mo, ^{94}Mo, ^{96}Ru and ^{98}Ru, p-process isotopes that exist in high abundance in the cosmos and are difficult to reproduce in previous nucleosynthesis models. Dauphas et al. (2003) pointed out that a critical test that models of p-process nucleosynthesis must pass is that they must reproduce the abundances of the short-lived nuclides ^{92}Nb and

^{146}Sm. In particular, ^{92}Nb provides strong constraints on p-process nucleosynthesis because it is shielded by ^{92}Mo from decays of proton-rich progenitor nuclides and thus cannot be produced by processes on the proton-rich side of the nuclear chart, such as the rp- or νp-processes.

We should note that the nature of SN Ia progenitors remains still uncertain. Following the idea of Li et al. (2011) and Jimenez et al. (2013), we supposed that at least 50% of SN Ia are single degenerate standard Chandrasekhar mass. But the reader has to keep in mind that they can be more rare. Referring to Ruiter et al. (2013) and Ruiter et al. (2014), population synthesis models tells us that SN Ia progenitors come from a (rare) sample of common-envelope phase binaries which may or may not undergo some s-processing before the explosion. If they do, the outcome would be pretty much the same as in the Chandrasekhar mass models and GCE results would not change so much with respect to what we presented in this paper. A detailed analysis of double degenerate scenario as well as mergers as SN Ia progenitors will be presented in a forthcoming paper.

Under the above conditions, we show here that SN Ia can reproduce the abundances of both ^{92}Nb and ^{146}Sm in meteorites within a factor of $\sim$2. The match would be poorer if solar system material had been isolated from fresh nucleosynthetic inputs for a long time.

A detailed investigation of nuclear uncertainties affecting the reaction rates producing and destroying ^{92}Nb, ^{92}Mo, and ^{146}Sm is presented. We found that the calculated ^{146}Sm/^{144}Sm ratio was compatible with the meteoritic value when using a ^{148}Gd(γ,α) rate based either on a fit to the Somorjai et al. (1998) (α,γ) cross sections or on the recent rate including an additional reaction channel as presented by Rauscher (2013). Concerning ^{92}Nb, the most important reactions affecting the ^{92}Nb/^{92}Mo ratio were discussed and the impact of their nuclear uncertainties explored. The ^{92}Nb/^{92}Mo ratio at 9.2 Gyr ranges between 1.66×10^{-5} and 3.12×10^{-5} due to the nuclear uncertainties. This demonstrates that the meteoritic value can be reproduced within these uncertainties. We conclude that SNIa can play a key role in explaining meteoritic abundances of the extinct radioactivities ^{92}Nb and ^{146}Sm but that nuclear uncertainties still have considerable impact.

We deeply thanks the anonymous referee for very usefull comments to this manuscript. This work has been supported by the B2FH Association. The numerical calculations have been supported by Regione Lombardia and CILEA Consortium through a LISA Initiative (Laboratory for Interdisciplinary Advanced Simulation) 2010 grant, and by R. Reifarth at Frankfurt Goethe University. CT thanks C. Arlandini, P. Dagna, and R. Casalegno for technical support in the simulations. TR is partially supported by the Swiss NSF, the European Research Council, and the THEXO collaboration within the 7^{th} Framework Programme of the EU. ND is supported by grants NNX12AH60G and NNX14AK09G from NASA. WH's work is supported by the German Science Foundation (DFG) through the Cooperative Research Center TRR33 'Dark Universe' and the Cluster of Excellence 'Origin and Structure of the Universe'. The work of FR is supported by the Emmy Noether program of the German Science Foundation (RO 3676/1-1), the ARCHES prize of the German Ministry of Education and Research (BMBF) and by the Nuclear Astrophysics Virtual Institute (VH-VI-417) of the Helmholtz Association.

REFERENCES

Arlandini, C., Käppeler, F., Wisshak, K., Gallino, R., Lugaro, M., Busso, M., & Straniero, O. 1999, ApJ, 525, 886

Arnould, M., & Goriely, S. 2006, Nucl. Phys. A, 777, 157

Bao, Z.Y., Beer, H., Käppeler, F., Voss, S., Wisshak, K., & Rauscher, T. 2000, Atomic Data and Nuclear Data Tables, Volume 76, 70-154

Becker, H., & Walker, R.J. 2003, Chemical Geology, 196, 43

Bennett, C.L., Larson, D., & Weiland, J.L. et al. 2013, ApJS, 208, 20

Bisterzo, S., Travaglio, C., Gallino. R., Wiescher, M., & Käppeler, F. 2014, ApJ, 787, 10

Borg, L.E., Brennecka, G.A., Marks, N.E., & Symes, S.J.K. 2014, in Lunar and Planetary Science Conference, 45, 1037

Boyet, M., Carlson, R.W., & Horan, M. 2010, Earth and Planetary Science Lett. 291, 172

Clayton, D.D. 1988, Montly Not. Royal Astron. Soc., 234, 1

Dauphas, N. 2005, Nature, 435, 1203

Dauphas, N., & Chaussidon, M. 2011, Annual Review of Earth and Planetary Sciences, 39, 351-386

Dauphas, N., Marty, B., & Reisberg, L. 2002, ApJ, 565, 640

Dauphas, N., Rauscher, T., Marty, B., & Reisberg, L. 2003, Nucl. Phys. A, 719, 287c

Davis, A.M., & McKeegan, K.D. 2013, Treatise on Geochemistry (Second Edition), Ed. Holland, Heinrich D. & Turekian, Karl K. (Elsevier), p. 361

Dillmann, I., Heil, M., Käppeler, F., Plag, R., Rauscher, T., & Thielemann, F.-K. 2006, AIP Conf. Proc. 819, 123; KADoNiS (Karlsruhe Database of Nucleosynthesis in Stars), available at `http://www.kadonis.org`

Dillmann, I., Domingo-Pardo, C., Heil, M., Käppeler, F., Walter, S., Dababneh, S., Rauscher, T., & Thielemann, F.-K. 2010, Phys. Rev. C 81, 015801

Friedmann, A.M. 1966, Radiochim. Acta, 5, 192

Gallino, R., Arlandini, C., Busso, M., Lugaro, M., Travaglio, C., Straniero, O., Chieffi, A., & Limongi, M. 1998, ApJ, 497, 388

Harper, C.L.Jr. 1996, ApJ, 466, 437

Hayakawa, T., Nakamura, K., Kajino, T., Chiba, S., Iwamoto, N., Cheoun, M.K., & Mathews, G.J. 2013, ApJ, 779, L9

Hoffman, R.D., Woosley, S.E., Fuller, G.M., & Meyer, B.S. 1996, ApJ, 460, 478

Howard, W.M., Meyer, B.S., & Woosley, S.E. 1991, ApJ, 373, L5

Howard, W.M., & Meyer, B.S. 1993, in Proceedings of the 2nd International Symposium on Nuclear Astrophysics, held at Karlsruhe, Germany. Ed. by F. Kaeppeler and K. Wisshak, (Bristol: IOP Publishing) p.575

Huss, G.R., Meyer, B.S., Srinivasan, G., Goswami, J.N., & Sahijpal, S. 2009, Geochimica et Cosmochimica Acta, 73, 4922

Iben, I.Jr. 1981, ApJ, 243, 987

Iben, I.Jr., & Tutukov, A.V. 1991, ApJ, 370, 615

Jacobsen, S.B., & Wasserburg, G.J. 1984, Earth Planet. Sci.Lett., 67, 137

Jacobsen, S.B. 2005, in Chondrites and the Protoplanetary Disk, vol. 341, p. 548

Kasen, D., Röpke, F.K., & Woosley, S.E. 2009, Nature, 460, 869

Kinoshita, N. et al. 2012, Science, 335, 1614

Kiss, G. G., et al. 2013, Phys. Rev. C, 88, 045804

Kusakabe, M., Iwamoto, N., & Nomoto, K. 2011, ApJ, 726, 25

Langanke, K., & Martínez-Pinedo, G. 2000, Nucl. Phys. A, 673, 481

Li, W., Chornock, R., Leaman, J., Filippenko, A.V., Pozmanski, D., Wang, X., Ganeshalingam, M., & Mannucci, F. 2011, MNRAS, 412, 1473

Lodders, K., Palme, H., & Gail, H.-P. 2009, Landolt-Börnstein - Group VI Astronomy and Astrophysics Numerical Data and Functional Relationships in Science and Technology, Edited by J.E. Trümper,4B: solar system, 4.4

Lugmair, G.W., & Marti, K. 1977, Planet. Sci. Lett., 35, 273

Lugmair, G.W., & Galer, S.J.G. 1992, Geochim. Cosmochim. Acta, 56, 1673

Marganiec, J., Dillmann, I., Domingo Pardo, C., Käppeler, F., & Walter, S. 2010, Phys. Rev. C 82, 035806

McWilliam, A. 1997, Annual Review of Astronomy & Astrophysics, 35, 503

Meissner, F., Schmidt-Ott, W.-D., & Ziegeler, L. 1987, Z. Phys. A, 327, 171

Meyer, B.S. 2003, Nucl. Phys. A, 719, 13c

Prinzhofer, A., Papanastassiou, D.A., & Wasserburg, G.J. 1989, ApJ, 344, L81

Prinzhofer, A., Papanastassiou, D.A., & Wasserburg, G.J. 1992, Geochim. Cosmochim. Acta 1992, 56, 797

Qian, Y.Z., Vogel, P., & Wasserburg, G.J. 1998, ApJ, 494, 285

Rauscher, T., & Thielemann, F.-K. 2000, Atomic Data Nucl. Data Tables, 75, 1

Rauscher, T. 2012, ApJS, 201, 26

Rauscher, T. 2013, Phys. Rev. Lett., 111, 061104

Rauscher, T. 2014, AIP Advances, 4, 041012

Rauscher, T., Thielemann, F.-K., & Oberhummer, H. 1995, ApJ, 451, L37

Rauscher, T., Thielemann, F.-K., & Kratz, K.-L. 1997, Phys. Rev. C, 56, 1613

Rauscher, T., Heger, A., Hoffmann, R.D., & Woosley, S.E. 2002, ApJ, 576, 323

Rauscher, T., Mohr, P., Dillmann, I., & Plag, R. 2011, ApJ, 738, 143

Rauscher, T., Dauphas, N., Dillmann, I., Fröhlich, C., Fülöp, Z., & Gyürky, G. 2013, Rep. Prog. Phys., 76, 66201

Rayet, M., Arnould, M., Hashimoto, M., Prantzos, N., & Nomoto, K. 1995, A&A, 298, 517

Ruiter, A., et al. 2013, MNRAS, 429, 1425

Ruiter, A.J., Belczynski, K., Sim, S.A., Seitenzahl, I.R., & Kwiatkowski, D. 2014, MNRAS, 440, L101

Schönbächler, M., Lee, D.-C., Halliday, A. N., Rehkäper, M., Hattendorf, B., Günther, D. 2002, Meteoritics & Planetary Science, vol. 37, Supplement, p.A127

Schramm, D.N., & Wasserburg, G.J. 1970, ApJ, 162, 57

Somorjai, E., et al. 1998, A&A, 333, 1112

Travaglio, C., Galli, D., Gallino, R., Busso, M., Ferrini, F., & Straniero, O. 1999, ApJ, 521, 691

Travaglio, C., Gallino, R., Arnone, E., Cowan, J., Jordan, F., & Sneden, C. 2004, ApJ, 601, 864

Travaglio, C., Gallino, R., Busso, M., & Gratton, R. 2001, ApJ, 549, L346

Travaglio, C., Hillebrandt, W., Reinecke, M., & Thielemann, F.-K. 2004, A&A, 425, 1029

Travaglio, C., Röpke, F.K., Gallino, R., & Hillebrandt, W. 2011, ApJ, 739, 93

Woosley, S.E., & Howard, W.M. 1978, ApJS, 36, 285

Woosley, S.E., & Howard, W.M. 1990, ApJ, 354, L21

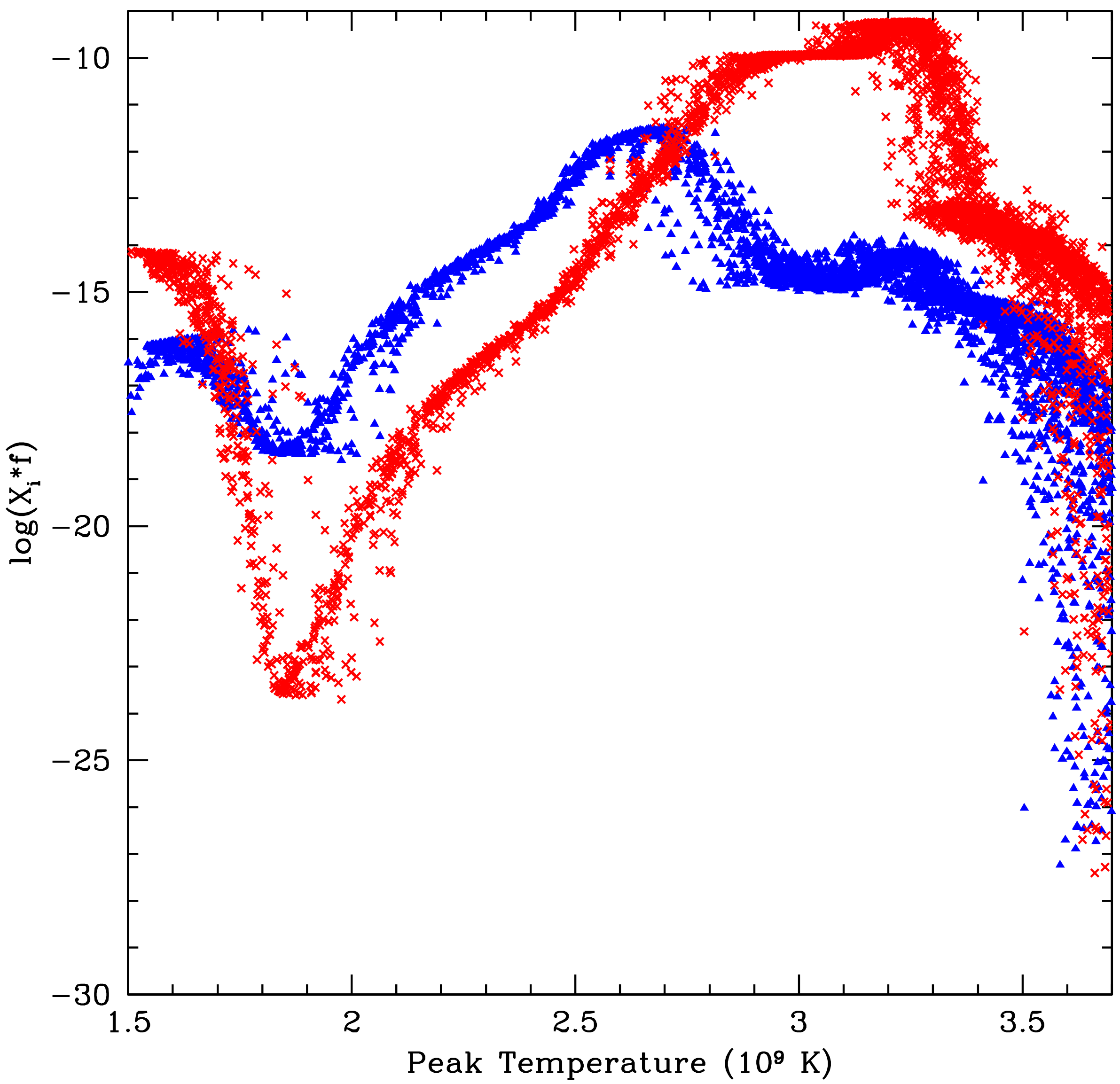

Fig. 1.— Abundance vs. T peak of the ratio ^{92}Nb and ^{92}Mo for tracers selected in the T range allowed for p-process nucleosynthesis. Each small dot represents one tracer. *Filled blue triangles* are for ^{92}Nb and *red crosses* are for ^{92}Mo. All the abundances X_i shown here and in the following Figures 2 and 3 are for an individual tracer, and the f factor in the plot is for $M_{\rm WD}(= 1.407\ \mathrm{M}_{\odot})/\mathrm{N}_{tracers}$ (=51200), i.e. the mass of each tracer.

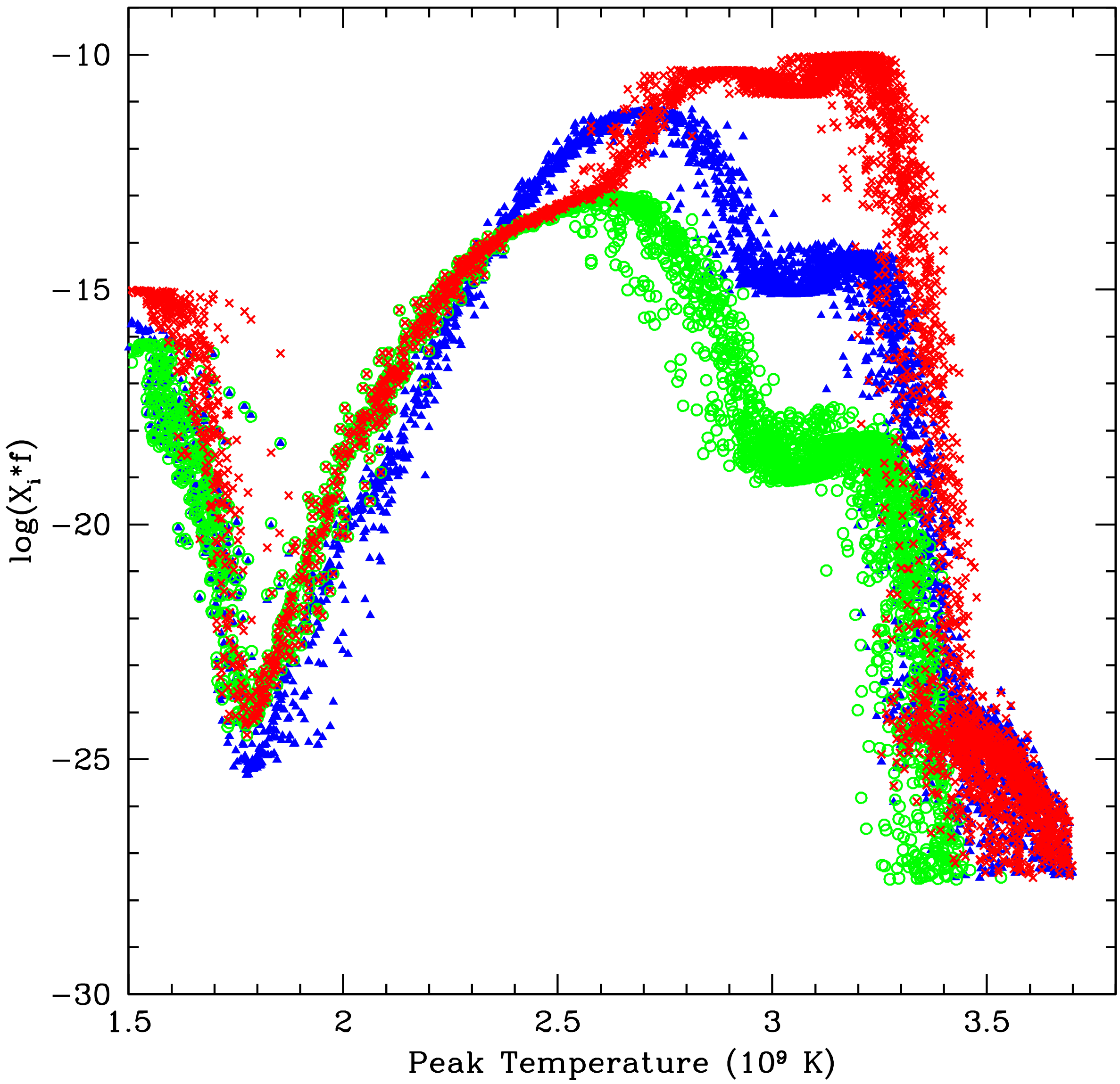

Fig. 2.— Same as Fig. 1, for ^{97}Tc (*filled blue triangles*), ^{98}Tc (*open green circles*) and ^{98}Ru (*red crosses*)

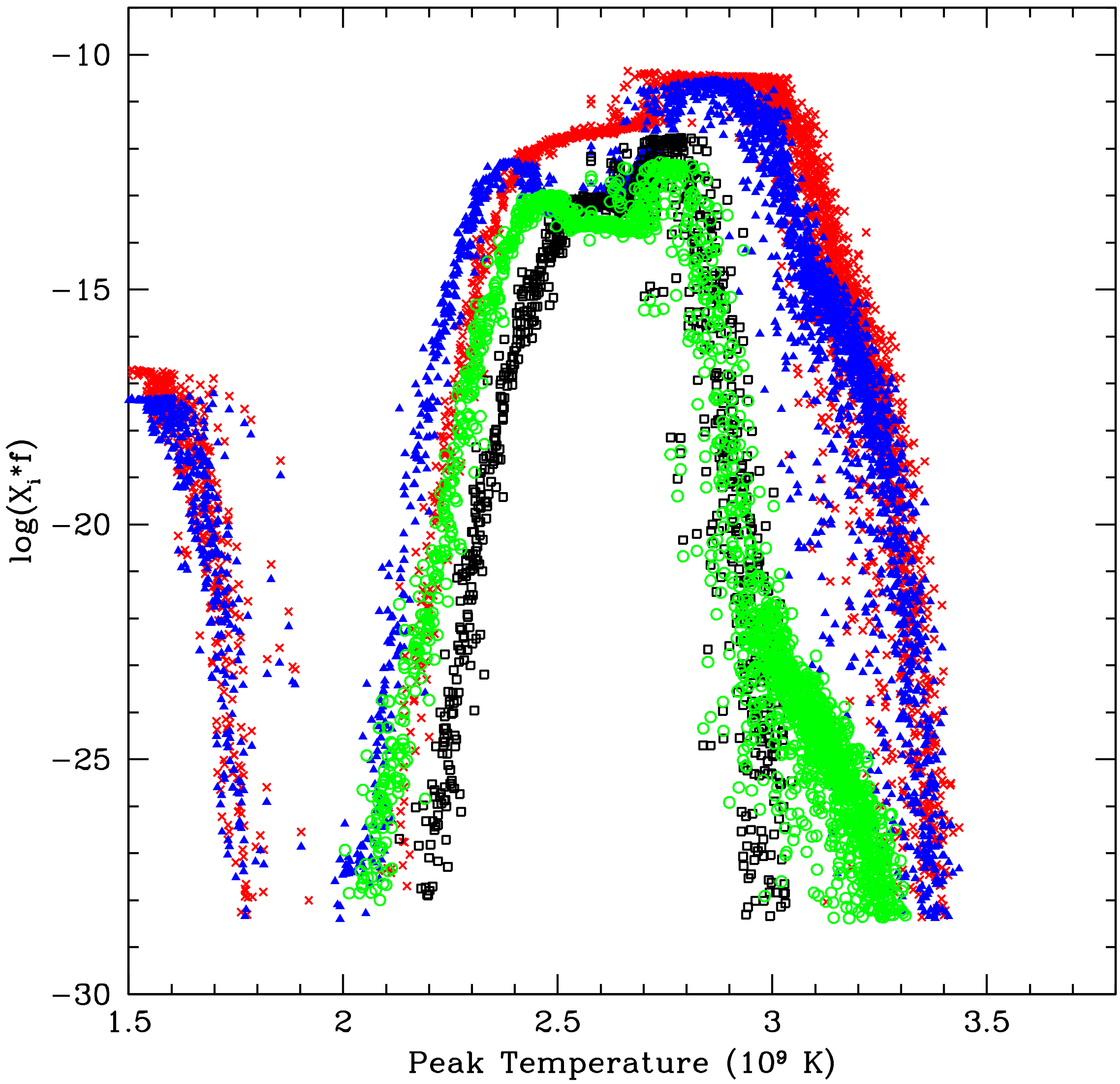

Fig. 3.— Same as Fig. 1, for ^{146}Sm (*filled blue triangles*), ^{150}Gd (*open green circles*), ^{154}Dy (*open black squares*) and ^{144}Sm (*red crosses*)

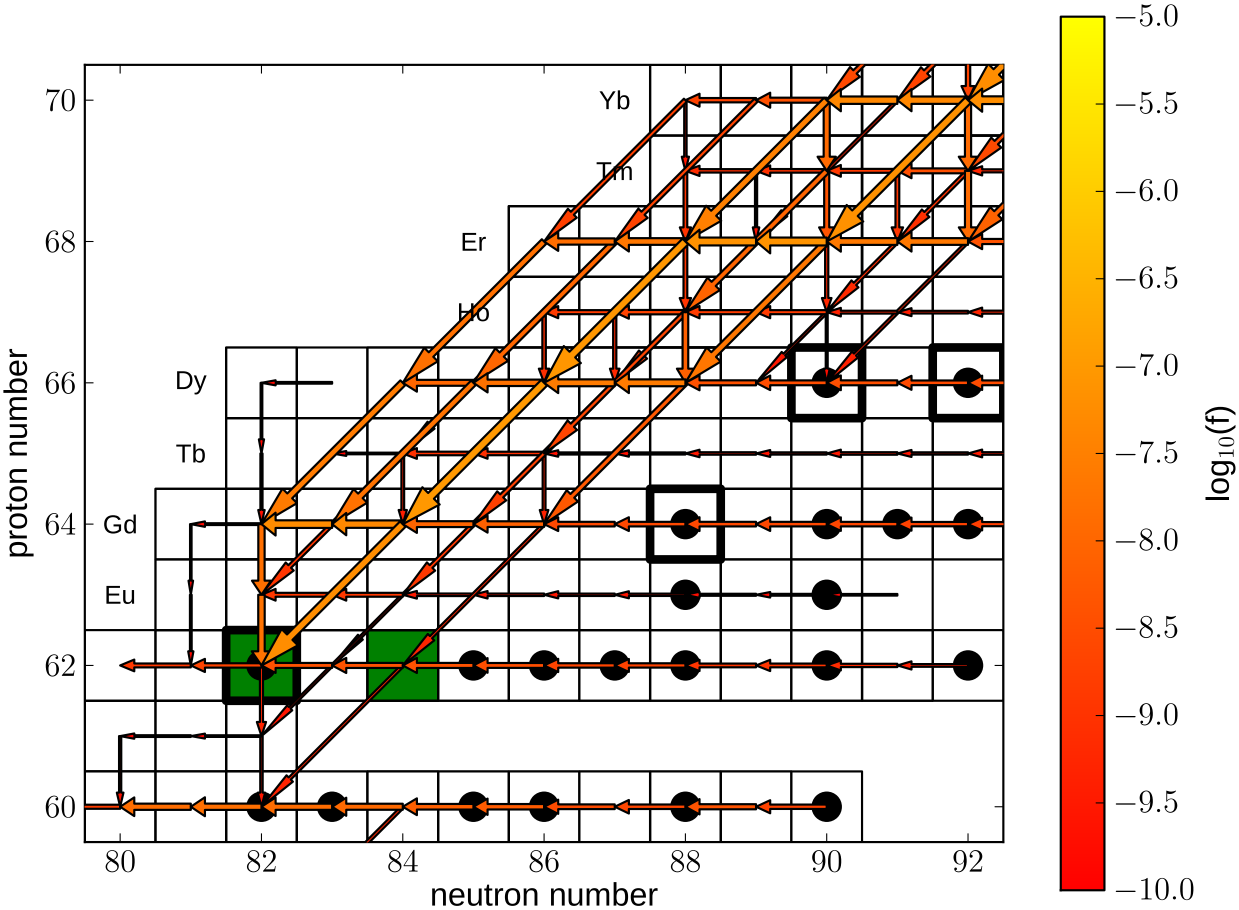

Fig. 4.— Reaction flow for ^{146}Sm production; size and color of the arrows relate to the magnitude of the time-integrated flux on a logarithmic scale. Stable isotopes are marked by a *black dot* and *p*-isotopes by a *thicker box*. The isotopes ^{144}Sm and ^{146}Sm are marked in *green*.

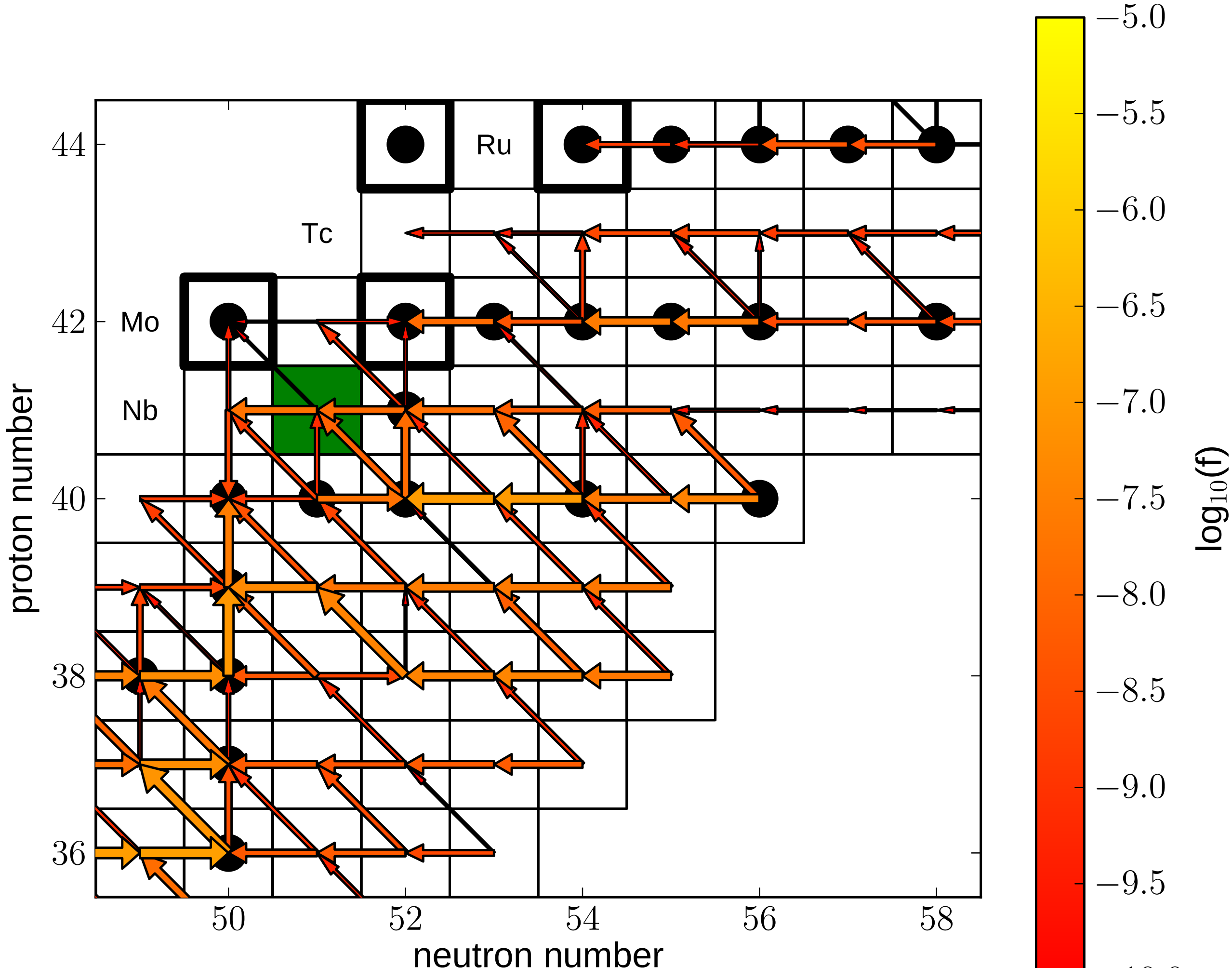

Fig. 5.— Reaction flow for ^{92}Nb production; size and color of the arrows relate to the magnitude of the time-integrated flux on a logarithmic scale. Stable isotopes are marked by a *black dot* and *p*-isotopes by a *thicker box*. The nuclide ^{92}Nd is marked in *green*.

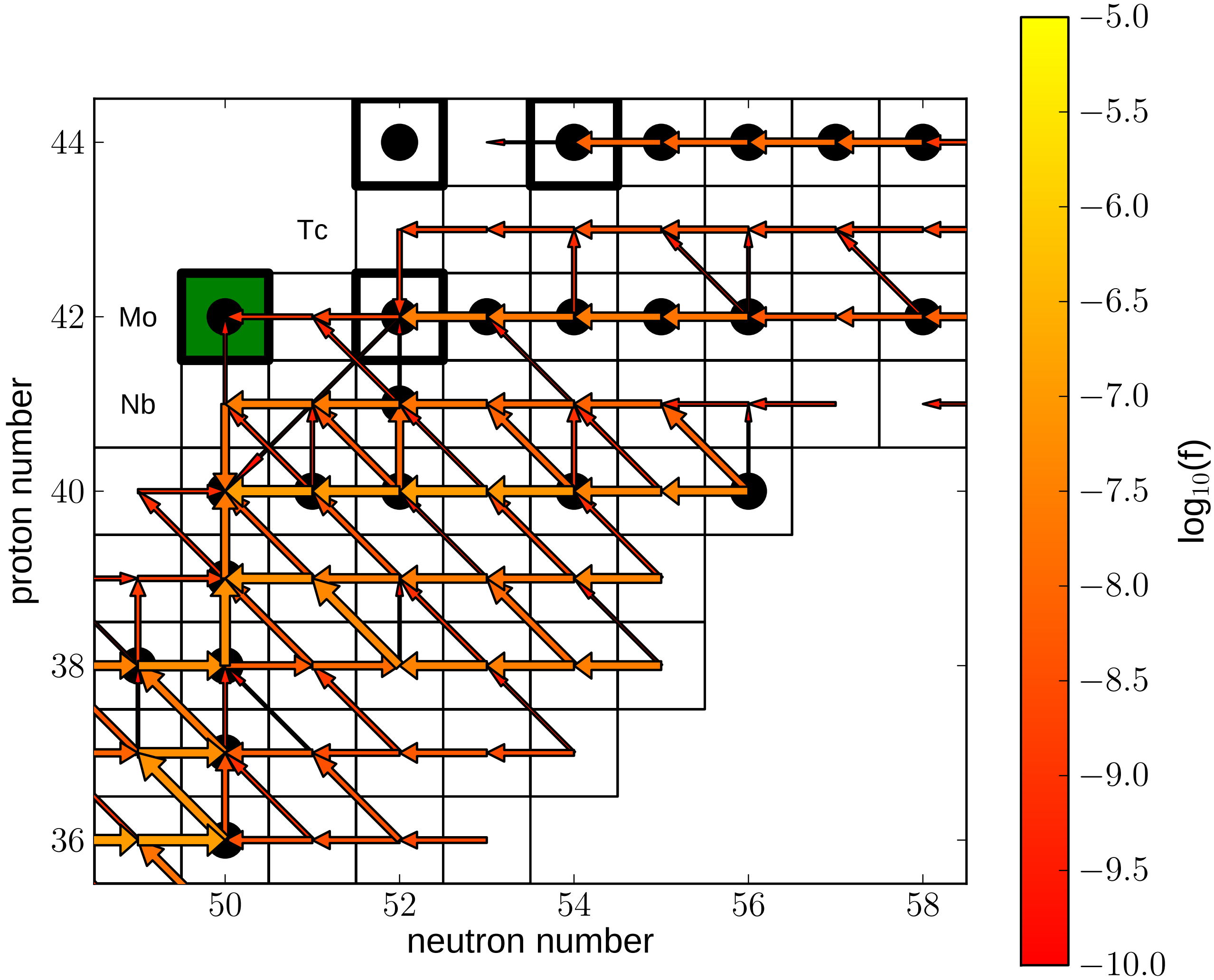

Fig. 6.— Reaction flow for ^{92}Mo production; size and color of the arrows relate to the magnitude of the time-integrated flux on a logarithmic scale. Stable isotopes are marked by a *black dot* and *p*-isotopes by a *thicker box*. The nuclide ^{92}Mo is marked in *green*.

Table 1. Radiogenic ratios at different metallicities

Ratio	Z=0.003	Z=0.006	Z=0.01	Z=0.012	Z=0.015	Z=0.02
^{92}Nb/^{92}Mo	7.363×10^{-4}	1.145×10^{-3}	1.526×10^{-3}	1.322×10^{-3}	1.846×10^{-3}	1.635×10^{-3}
^{97}Tc/^{98}Ru	1.215×10^{-2}	1.767×10^{-2}	2.354×10^{-2}	2.406×10^{-2}	2.533×10^{-2}	2.285×10^{-2}
^{98}Tc/^{98}Ru	8.465×10^{-5}	1.798×10^{-4}	3.384×10^{-4}	3.711×10^{-4}	4.741×10^{-4}	5.066×10^{-4}
^{146}Sm/^{144}Sm	4.053×10^{-1}	3.705×10^{-1}	3.624×10^{-1}	3.762×10^{-1}	3.329×10^{-1}	3.161×10^{-1}

Table 2. Galactic chemical evolution of radiogenic isotopes

[Fe/H]	Age (Gyr)	^{92}Nb/^{92}Mo	^{97}Tc/^{98}Ru	^{98}Tc/^{98}Ru	^{146}Sm/^{144}Sm
-1	1.57	1.700×10^{-4}	1.752×10^{-5}	2.582×10^{-6}	4.209×10^{-2}
-0.8	2.14	1.298×10^{-4}	2.851×10^{-4}	1.953×10^{-6}	3.244×10^{-2}
-0.5	3.50	8.344×10^{-5}	1.778×10^{-4}	1.557×10^{-6}	2.039×10^{-2}
-0.3	4.80	6.515×10^{-5}	1.561×10^{-4}	2.005×10^{-6}	2.457×10^{-2}
-0.155	6.20	4.033×10^{-5}	1.018×10^{-4}	1.432×10^{-6}	1.807×10^{-2}
0.0	9.20	$\mathbf{1.752\times10^{-5}}$	$\mathbf{4.077\times10^{-5}}$	$\mathbf{6.471\times10^{-7}}$	$\mathbf{6.989\times10^{-3}}$
0.092	11.7	1.137×10^{-5}	2.681×10^{-5}	4.803×10^{-7}	4.644×10^{-3}
	Meteoritic	$(2.8\pm0.5)\times10^{-5}$	$< 4.0\times10^{-4}$	$< 2.0\times10^{-5}$	$(9.4\pm0.5)\times10^{-3}$

Table 3. Dependence of the ^{146}Sm/^{144}Sm ratio on various ^{148}Gd(γ,α) rates for SNIa at different metallicities and (last line) for GCE calculations.

Z	RATH[a]	exp (α,γ) fit[b]	2013[c]
0.003	4.053×10^{-1}	7.408×10^{-1}	9.76×10^{-1}
0.006	3.705×10^{-1}	7.097×10^{-1}	8.90×10^{-1}
0.01	3.624×10^{-1}	6.850×10^{-1}	8.74×10^{-1}
0.012	3.762×10^{-1}	6.651×10^{-1}	9.05×10^{-1}
0.015	3.329×10^{-1}	6.319×10^{-1}	8.01×10^{-1}
0.02	3.161×10^{-1}	6.132×10^{-1}	7.62×10^{-1}
GCE τ=68 Myr	6.989×10^{-3}	1.050×10^{-2}	1.667×10^{-2}

[a]Rauscher & Thielemann (2000)

[b]Somorjai et al. (1998)

[c]Rauscher (2013)

Table 4. Reactions affecting the ^{92}Nb/^{92}Mo ratio and their variation to explore the nuclear uncertainties; rate set MIN yields the minimal ratio, set MAX the maximal ratio. The arrows indicate whether a rate has been multiplied by a factor of two (arrow up) or divided by the same factor (arrow down). The modifications always apply to the rate and its reverse rate. In the last line there are the GCE calculations with these assumptions.

Reactions	Rate set MIN	Rate set MAX
^{91}Zr(p,γ)^{92}Nb	$\downarrow$	$\uparrow$
^{92}Zr(p,γ)^{93}Nb	$\downarrow$	$\uparrow$
^{92}Zr(p,n)^{92}Nb	$\downarrow$	$\uparrow$
^{91}Nb(n,γ)^{92}Nb	$\uparrow$	$\downarrow$
^{92}Nb(n,γ)^{93}Nb	$\downarrow$	$\uparrow$
^{91}Nb(p,γ)^{92}Mo	$\uparrow$	$\downarrow$
^{93}Nb(p,n)^{93}Mo	$\uparrow$	$\downarrow$
^{93}Mo(n,γ)^{94}Mo	$\uparrow$	$\downarrow$
GCE	1.660×10^{-5}	3.118×10^{-5}